View metadata, citation and similar papers at core.ac.uk
brought to you by CORE
provided by Nottingham ePrints

Influence of Surface Passivation on Indium Arsenide Nanowire Band Gap Energies

Razavi, P, Greer, J.C.

University of Nottingham
UK | CHINA | MALAYSIA

University of Nottingham Ningbo China, 199 Taikang East Road, Ningbo, 315100, China

First published 2019

This work is made available under the terms of the Creative Commons Attribution 4.0 International License:
http://creativecommons.org/licenses/by/4.0

The work is licenced to the University of Nottingham Ningbo China under the Global University Publication Licence:

https://www.nottingham.edu.cn/en/library/documents/research-support/global-university-publications-licence.pdf

University of Nottingham

UK | CHINA | MALAYSIA

Influence of Surface Passivation on Indium Arsenide Nanowire Band Gap Energies

Pedram Razavi[1] and James C. Greer[2*]

[1]Tyndall National Institute, University College Cork, Lee Maltings, Dyke Parade, Cork T12 R5CP, Ireland

[2]University of Nottingham Ningbo New Materials Institute and Department of Electrical and Electronic Engineering, University of Nottingham Ningbo China, 199 Taikang East Road, Ningbo 315100, China

[*] Corresponding author: jim.greer@nottingham.edu.cn

Abstract

The interplay between surface chemistry and quantum confinement on the band gap energies of indium arsenide (InAs) nanowires (NWs) is investigated by first principle computations as the surface-to-volume ratio increases with decreasing cross section. Electronic band structures are presented as determined by both density functional and hybrid density functional theory (DFT) calculations; the latter are used to provide improved band gap energy estimates over those from standard approximate DFT methods. Different monovalent chemical species with varying electron affinity are used to eliminate surface states to enable direct comparison between surface chemistry and quantum confinement. The influence of these effects on energy band gaps and electron effective masses is highlighted. It is found that many desirable properties in terms of electronic properties and the elimination of surface states for nanoscale field effect transistors fabricated using [100]-oriented InAs can be achieved.

1. Introduction

Group III - group V (III-V) compound semiconductors can provide improved performance for key properties of ultra-scaled transistors used in complementary metal oxide semiconductor (CMOS) integrated circuits [1, 2], emerging electronics [3], optoelectronics [4], sensing, and energy harvesting [5]. The development of 7 nm and 5 nm technology nodes are currently being pursued for the next generation of integrated circuits [6-8] and accepted wisdom points to advanced semiconductor technologies requiring semiconductor 'fin' field effect

transistor (finFET) or nanowires (NWs) with critical dimension well below sub-10 nanometer widths. As a transistor's channel becoming increasingly smaller, short channel effects arise leading to an increasing migration towards NW transistors with gate-all-around configurations to reduce short channel effects such as drain-induced barrier lowering (DIBL) and to increase subthreshold current swing through greater electrostatic control of the channel [9]. Advances in top down and bottom up fabrication techniques are leading to reproducible fabrication techniques for NWs with diameters as small as 1 nm [10-12]. At these length scales bulk properties do not accurately describe a NW's electronic structure as quantum confinement effects become pronounced, and as well the increase in the surface-to-volume ratio results in the surface strongly influencing electronic properties. It is known for small non-polar semiconductor NWs with small cross sectional areas that surface chemistry significantly modifies energy band gaps and electronic properties. Accurate descriptions of the electronic structure in these cases require specific studies at different NW cross sectional areas with differing terminating species [13, 14]. To explore the interplay between the quantum confinement and surface chemistry for III-V nanowires, electronic structures are studied for gallium arsenide (GaAs) and indium arsenide (InAs) NWs. The primary emphasis is for InAs NWs which due to its small band gap, high electron mobility, and large injection velocity makes this III-V material a promising candidate for the beyond-the-silicon roadmap devices [11].

2. Methods

First principles calculations allow explicit treatment of the effects arising from quantum confinement and surface chemistry on the electronic properties and hence implicitly the electrical behavior of NWs. The calculations reported here are all performed with the Vienna Ab-initio Simulation Package (VASP) [15-17]. DFT/GGA calculations are performed using the Pedrew-Burke-Ernzerhof (PBE) exchange-correlation functional [18] with the projected augmented wave method [19,20]. Hybrid DFT calculations are performed using a screened exchange HSE06 functional [21] with 25% exact exchange and a screening length of 0.2 Å^{-1}. The hybrid DFT calculations are performed to provide better estimates for band gap energies by relying on mixing in exact exchange to compensate for the well-known deficiencies related to electronic structures using the DFT/GGA approximation. A plane wave cut-off energy of 460 eV is chosen with a $11\times1\times1$ k-point grid used to converge the electronic energy. The lattice parameters along

the NW axe and atomic positions are optimized leading to all residual forces being less than 10 meV/Å per atom.

Due to the underlying polar nature of the III-V lattice, NWs with different principle axis orientations typically present surface facets with a more elaborate surface chemistry as compared to non-polar semiconductors [22]. As a result and as well-known to researchers and technologists in this field, surface passivation of III-V semiconductors is more difficult to achieve compared to silicon surfaces. This has historically hindered the use of III-V materials in metal-oxide-semiconductor FETs (MOSFETs) due to the resulting fixed charge distribution at the semiconductor-oxide interface leading to screening of the gate electric field [23]. Many experimental investigations for III-V NWs have been performed but diameters typically are much larger than the 10 nanometer upper limit required for advanced nanoelectronics geometries [24-26]. Theoretical studies of III-V NWs have typically considered unterminated NWs, idealized surface terminations using pseudo-hydrogen, or considering only a single atomic species for surface passivation [27-30].

In vapour-liquid-solid phase (VLS) epitaxial growth, NWs with hexagonal cross sections are mainly produced. In the grown NWs, both zinc blende and wurtzite structures can be found although through control of growth conditions either phase can be stabilized [31]. For VLS-grown zinc blende NWs, [111] oriented NWs with $\{11\bar{2}\}$ and $\{\bar{1}10\}$ surface facets are the most commonly produced structures. As has been shown for GaAs NWs with the zinc blende structure, these surface facets can be passivated with hydrogen termination [32]. It will be demonstrated that this remains true for the InAs surfaces too.

For nanoelectronics, epitaxial growth of NWs is less common than growth of an epitaxial layer followed by top down patterning consisting of photolithography and etching steps, particularly for finFET structures. For the deposited films, the zinc blende phase is commonly found to be the more stable phase. The surface facets are determined by the growth direction and the orientation of the deposited patterns relative to the in-plane orientation of the film. Following patterning, non-equilibrium or metastable structures result and the surface facets that are created can be anion-rich, cation-rich or display a comparable numbers of cations and anions. It will be demonstrated for the monovalent terminating species considered within this study, electron counting (EC) rules apply and that not all surface facets can be terminated with the monovalent chemistry chosen. This adds another design constraint when engineering top down finFET and NW transistors.

GaAs surface reconstructions give rise to Ga dangling bonds, As dangling bonds, Ga dimers, and As dimers. The energies from these atomic configurations relative to the Fermi level provide insight to which levels must be eliminated. These conditions define the EC rules that when followed provide chemically passivated surfaces that are charge neutral, in analogy to the 3/4 and 5/4 charge balance rules leading to charge neutrality for bulk sp^3 bonding [23]. An ideal As-terminated (100) surface is electron rich and a termination scheme using alumina Al_2O_3 has been proposed [23]. In contrast, As-terminated or In-/Ga-terminated surfaces cannot easily be passivated with the surface chemistries chosen for this study due to their formal charge states not being capable of matching the excess/deficit of electrons at these surfaces. The consequence is unpassivated surfaces displaying energy levels in the NW band gap for these cases.

The specific surface chemistries considered are: pseudo-hydrogen (-pseudo-H); hydrogen (-H); an amino group ($-NH_2$); and fluorine (-F). Pseudo-hydrogen atoms are fictional atom types commonly used in theoretical studies for surface passivation of III-V materials [33]. Their use allow the EC rules needed to balance the differing valences of the group III and group V atoms at a surface to be easily satisfied. This is achieved by formally changing the charge state of the pseudo-H atoms to non-integer or fractional values to saturate surface bonds. The use of pseudo-hydrogen thus eliminates complications associated with electronic states directly attributable to III-V surfaces and III-V/oxide interfaces that do not satisfy the EC rules using simple surface chemistries. Each pseudo-hydrogen atom is assigned a fractional atomic charges to allow for termination for either group III or group V atoms surface dangling bonds while taking into account variations in an atom's valence state due to local bonding configurations arising at surfaces or interfaces. The same pseudo-H fractional charges can be used to passivate either the GaAs or InAs NWs that are obtained by interchanging gallium with indium atoms, however each NW is relaxed independently to obtain zero strain structures. III-V materials terminated in this idealized way can readily be passivated through eliminating levels associated with a surface/interface that lie energetically within the energy band gap of the nanowire core [34]. For this study, the idealized pseudo-hydrogen terminated NWs act as a reference point to which the chemically (non-ideal) terminated surfaces can be compared.

NWs with square cross sections with sides in the length range between 1 nm to 3 nm are allowed to relax (energy optimization with respect to the atomic positions) within DFT calculations using both the generalized gradient

approximation (GGA) as well as DFT calculations with a hybrid exchange-correlation functional that empirically mixes exact exchange. From the NW models, electronic structures are examined and energy band gaps and the effective masses from the lowest lying energy valleys are extracted. This procedure is repeated for each NW orientation, cross section, and surface termination.

3. Results

Fig. 1 shows the atomic structure for the NWs with principle axe in the [100], [110] and [111] directions. Representative surface facets that can be chosen when creating the structures following patterning and etch steps are also labelled within fig. 1. It is well known for III-V materials that the (110) plane can be constructed as non-polar [22]. Hence for the [100] oriented NWs if the surfaces are selected as {110}, it is found that monovalent terminations are capable of saturating all the surface bonds.

However NWs with [110] and [111] orientations the ability to generate non-polar surfaces is not easily or is impossible to accomplish leading to surface facets with differing amounts of group III and group V atoms. As a consequence, the EC rules cannot in general be strictly satisfied using monovalent terminating species. Both the [110]- and [111]-oriented NWs yield surface facets with differing numbers of group III and group V atoms: this includes the (001) surface for [110]-oriented NWs and the $(1\bar{1}2)$ surface for [111] -oriented NWs. The (001) surface for the [110]-oriented NWs leads to either all anions or all cations at the semiconductor surface. As a result, the [110]-oriented NWs could not be passivated and during the structure optimization, the atoms/molecules introduced to passivate dangling bonds dissociate from the surface. This results is from the excess/deficit of electrons on these surfaces and the fact that only monovalent terminating species are introduced leading to a situation where the EC rules cannot even be approximately satisfied. The (112) surface for the [111]-oriented NWs contain both cations and anions but in unequal numbers. Nonetheless, the [111]-oriented NWs could be successfully passivated. This is achieved although the (112) surface facets of the [111]-oriented NWs contain both cations and anions in differing ratios (one facet contain 65% anions and 35% cations, whereas the other contains 35% anions and 65% cations; see fig. S1 in the supplementary

material for the side views of these NWs). This finding is consistent with what is observed for the passivation of epitaxially grown NWs by hydrogen.

The electronic structure of the passivated NWs are explored in terms of band folding and compared relative to the pseudo-hydrogen or idealized terminated surfaces in terms of energy band gaps and effective masses for the lowest energy conduction band valleys. As is usual for NWs with less than 5 nm critical dimensions, band folding results in significantly different electronic structure properties relative to the same material in bulk form, and for example the direct/indirect nature and magnitude of the band gap can change. The direct/indirect nature of the band gap is crucial for photonic device design when accompanied by strong dipole coupling matrix elements at the direct gap. Equally, the energy band gap plays a central role for nanoelectronic applications as the magnitude of the band gap determines operating voltages, the thermal operation for semiconductor transistors, and controls source-to-drain tunnelling in field effect transistors [12, 22].

As seen in fig. 2, the electronic structure is heavily dependent on the III-V material choice as well as NW orientation. Figs. 2(a) and 2(b) illustrate the band structure an approximately 1.6 x 1.6 nm^2 cross section [100]-oriented GaAs and a 2.0 x 2.0 nm^2 cross section [100]-oriented InAs NWs, both terminated by hydrogen. In both cases, it is found that ideal electrical passivation of the surface can be achieved as reflected by the (site-)projected electronic density of states (PDoS) which reveals no energy levels within the NWs' band gaps (see fig. S2 in the supplementary material) suggesting some degree of transferability in relation to surface passivation between GaAs and InAs. As previously mentioned, the [100]-oriented NWs are easily passivated due to the ability to identify facets with an equal number of group III and group V atoms on the surfaces. The band structure for an approximately 3 nm x 3 nm cross section [111]-oriented InAs NWs is shown in fig. 2(c) with hydrogen termination and as shown, ideal passivation is likewise achieved in the sense there are no surface induced states at the conduction or valence band edges as shown by a PDoS analysis. From the PDoS, it is found that there are no surface-related energy levels within the band gap (see fig. S3 in supplementary material).

The effect of the different terminating species on electronic structure for ultra-thin InAs NWs with sides of length of 1.2 nm with a principal axis along the [100]-orientation is shown in fig. 3. It can be seen that the introduction of surface terminations with differing electronegativity results in passivation of surface

states for all cases with the -F termination resulting in the narrowest band gap and the $-NH_2$ being intermediate, and with hydrogen and pseudo-hydrogen resulting in the largest band gap energies. This trend is also observed for the larger NWs investigated as shown in fig. 4 revealing a lowering of the magnitude of the band gap energy with increasing electronegativity.

Band gap energies and conduction band effective masses for the different InAs NW cross sections are extracted and summarized from the electronic band structures in fig. 4(a) and 4(b). From fig. 4(a) it is clearly seen that the band gap energy differences with changing surface termination become larger with decreasing NW cross section as the surface-to-volume ratio increases.

The calculated effective mass for the -F terminated [100]-oriented InAs NW (with approximately 1.2 nm length along each side of the wire's cross section) is about 2 to 2.5 times smaller than those for the $-NH_2$ and -H terminated InAs NWs as shown in fig. 4(b). This would suggest a much higher electron mobility for -F terminated [100]-oriented InAs NWs with the corresponding band structure shown in fig. 3(d). At these dimensions, quantum confinement leads to a larger band gap relative to bulk InAs suitable for room temperature electronics. The increased band gap and due to the ability to reduce the electron effective mass by introducing surface bonds with large electronegativity, indicate near atomic limits to scaling that InAs remains an attractive choice for *n*-type MOSFETs in terms of the key electrical parameters that determine device operation.

The well-known band gap under-estimation of DFT/GGA calculations results in a zero band gap prediction for the $3 \ x \ 3 \ nm^2$ F-terminated InAs NW. However, corrections to the exchange-correlation energy using the hybrid functional results in what is anticipated to be a more accurate band gap estimate are shown in fig. 4(a). Notwithstanding the differences in the total band gap energies between the two approximations, the predicted trends in the band gap energies for differing surface electronegativity are similar from both the DFT/GGA and hybrid DFT predictions. Due to large quantum confinement effects arising at the extremely small cross section for these NWs, there is in all cases a substantial increase in the band gaps relative to the bulk energy gap. However, the band gap widening is not as large in -F and $-NH_2$ terminated NWs as that found for -H and -pseudo-H terminated NWs. This is due to the competition between quantum confinement and hybridization of the surface termination with the III-V NW valence band as indicated by the PDoS shown in fig. 5. Similar effects have also been observed

in ultra-thin silicon NWs [13,14] with narrowing of the band gap with increasing electronegativity of the surface terminating species.

The PDoS plotted in fig. 5 allows for a partitioning of the contributions from energy contributions derived from the passivating surface species and the semiconducting core of the InAs NWs. By considering the partial atomic contributions deriving either from the InAs NW or the surface terminations, it is seen that pseudo-H and -H terminated NWs have relatively small contributions to the DoS near the valence band edge. On the other hand for -NH_2 and -F terminated NWs, there is a significant number of states derived from the -NH_2 and -F surface atoms reflecting and increased hybridization with states originating from the valence band edge. States from the terminating species interact with those from In and As atoms at the surface and reduce the band gap through the splitting accompanying hybridization shown in fig. 5. This effect becomes increasingly pronounced as critical dimensions are reduced below 5 nm.

4. Conclusions

Design issues arising for III-V nanowires for ultra-thin InAs NW transistors have been examined theoretically using DFT to determine electronic band structures. During epitaxial growth of III-V NWs, growth kinetics largely determine the growth direction and which surface facets are present. For nanoelectronics applications such as for finFET devices, it is more common to grow an epitaxial thin film and to use photolithography to pattern to create 'fin' or NW structures. Using top down fabrication techniques can leads to consideration of the growth direction of the film which determines the top/bottom facets of a NW with controlled growth or deposition with the orientation of patterned structures with respect to the film determining the NW orientation as well as the sidewall surface facets. Considerations for selecting nanowires geometries that present facets which can be readily passivated and result in desirable electronic properties for ultra-scale nanoelectronics are described. Through consideration of the EC rules and by comparison to GaAs NWs, it is verified that many considerations in choosing a surface chemistry yielding a passivated surface may be transferred to the study of InAs NWs.

In general, band gaps for semiconductor NWs are significantly modified with the energy increasing substantially with decreasing NW cross sectional area due to quantum confinement. It is shown how varying surface terminations for InAs

NWs using pseudo-H, -H, $-NH_2$ and -F chemical species influence the electronic structure for small NW cross sectional areas. The increase in band gap for ultra-scale InAs NWs may be adjusted by selecting the electronegativity of the surface termination. The choice of surface terminations with larger electronegativity results in increased hybridization with the NW valence states resulting in a relative reduction in the energy band gap.

Electron effective masses increase with decreasing NW cross sectional area signalling a trade-off between reducing mobility and increasing electron carrier density. However, the [100]-oriented NWs can be readily passivated due to the identification of nonpolar surface facets which are readily passivated. This can be achieved with a band gap energy suitable for room temperature electronics while yielding an electron effective mass at the conduction band minimum suitable for high mobility charge transport. These properties reveal that [100]-oriented InAs NWs are strong candidates for high-performance *n*-type MOSFET channels fabricated near atomic scale limits.

Acknowledgments

This work was supported by the European Union project DEEPEN funded under NMR-2013-1.4-1 grant agreement number 604416. We also wish to acknowledge the SFI/HEA Irish Centre for High-End Computing (ICHEC) for the provision of computational facilities. JG acknowledges funding from the Nottingham Ningbo New Materials Institute.

References

1. Jesús A Del Alamo, *Nature* 2011, vol. 479, p. 317. ;
2. Adrian M Ionescu and Heike Riel, *nature* 2011, vol. 479, p. 329.
3. Junghyo Nah, Hui Fang, Chuan Wang, Kuniharu Takei, Min Hyung Lee, E Plis, Sanjay Krishna and Ali Javey, *Nano letters* 2012, vol. 12, pp. 3592-3595.
4. Peter J Pauzauskie and Peidong Yang, *Materials today* 2006, vol. 9, pp. 36-45.
5. SF Karg, V Troncale, U Drechsler, P Mensch, P Das Kanungo, H Schmid, V Schmidt, L Gignac, H Riel and B Gotsmann, *Nanotechnology* 2014, vol. 25, p. 305702.
6. S. Y. Wu, C. Y. Lin, M. C. Chiang, J. J. Liaw, J. Y. Cheng, S. H. Yang, C. H. Tsai, P. N. Chen, T. Miyashita, C. H. Chang, V. S. Chang, K. H. Pan, J. H. Chen, Y. S. Mor, K. T. Lai, C. S. Liang, H. F. Chen, S. Y. Chang, C. J. Lin, C. H. Hsieh, R. F. Tsui, C. H. Yao, C. C. Chen, R. Chen, C. H. Lee, H. J. Lin, C. W. Chang, K. W. Chen, M. H. Tsai, K. S. Chen, Y. Ku and S. M. Jang, In *2016 IEEE International Electron Devices Meeting (IEDM)*, (2016), pp 2.6.1-2.6.4;
7. R. Xie, P. Montanini, K. Akarvardar, N. Tripathi, B. Haran, S. Johnson, T. Hook, B. Hamieh, D. Corliss, J. Wang, X. Miao, J. Sporre, J. Fronheiser, N. Loubet, M. Sung, S. Sieg, S. Mochizuki, C. Prindle, S. Seo, A. Greene, J. Shearer, A. Labonte, S. Fan, L. Liebmann, R. Chao, A. Arceo, K. Chung, K. Cheon, P. Adusumilli, H. P. Amanapu, Z. Bi, J. Cha, H. C. Chen, R. Conti, R. Galatage, O. Gluschenkov, V. Kamineni, K. Kim, C. Lee, F. Lie, Z. Liu, S. Mehta, E. Miller, H. Niimi, C. Niu, C. Park, D. Park, M. Raymond, B. Sahu, M. Sankarapandian, S. Siddiqui, R. Southwick, L. Sun, C. Surisetty, S. Tsai, S. Whang, P. Xu, Y. Xu, C. Yeh, P. Zeitzoff, J. Zhang, J. Li, J. Demarest, J. Arnold, D. Canaperi, D. Dunn, N. Felix, D. Gupta, H. Jagannathan, S. Kanakasabapathy, W. Kleemeier, C. Labelle, M. Mottura, P. Oldiges, S. Skordas, T. Standaert, T. Yamashita, M. Colburn, M. Na, V. Paruchuri, S. Lian, R. Divakaruni, T. Gow, S. Lee, A. Knorr, H. Bu and M. Khare, In *2016 IEEE International Electron Devices Meeting (IEDM)*, (2016), pp 2.7.1-2.7.4;
   T. Huynh-Bao, S. Sakhare, J. Ryckaert, D. Yakimets, A. Mercha, D. Verkest, A. V. Y. Thean and P. Wambacq, In *2015 International Conference on IC Design & Technology (ICICDT)*, (2015), pp 1-4.
9. Jean-Pierre Colinge, James C Greer and Jim Greer: *Nanowire transistors: physics of devices and materials in one dimension*. (Cambridge University Press, 2016).
10. D. D. D. Ma, C. S. Lee, F. C. K. Au, S. Y. Tong and S. T. Lee, *Science* 2003, vol. 299, pp. 1874-1877.
11. Kyooho Jung, Parsian K Mohseni and Xiuling Li, *Nanoscale* 2014, vol. 6, pp. 15293-15300. ;
12. Pedram Razavi and James C. Greer, *Solid-State Electronics* 2018, vol. 149, pp. 6-14.
13. Leu, P. W.; Shan, B.; Cho, K., Phys. Rev. B 2006, **73**, 195320
14. Michael Nolan, Sean O'Callaghan, Giorgos Fagas, James C. Greer and Thomas Frauenheim, *Nano Letters* 2007, vol. 7, pp. 34-38.
15. G. Kresse and J. Hafner, *Physical Review B* 1993, vol. 47, pp. 558-561. ;
16. G. Kresse and J. Furthmüller, *Computational Materials Science* 1996, vol. 6, pp. 15-50. ;
17. G. Kresse and J. Furthmüller, *Physical Review B* 1996, vol. 54, pp. 11169-11186.
18. John P. Perdew, Kieron Burke and Matthias Ernzerhof, *Physical Review Letters* 1996, vol. 77, p. 3865-3868.
19. P. E. Blöchl, *Physical Review B* 1994, vol. 50, pp. 17953-17979. ;
20. G. Kresse and D. Joubert, *Physical Review B* 1999, vol. 59, pp. 1758-1775.
21. J. Paier, M. Marsman, K. Hummer, G. Kresse, I. C. Gerber and J. G. Ángyán, *The Journal of Chemical Physics* 2006, vol. 124, p. 154709.
22. Pedram Razavi and James C. Greer, *Materials Chemistry and Physics* 2018, vol. 206, pp. 35-39.
23. Liang Lin and John Robertson, *Journal of Vacuum Science & Technology B, Nanotechnology and Microelectronics: Materials, Processing, Measurement, and Phenomena* 2012, vol. 30, p. 04E101.

24. MH Sun, Hannah J Joyce, Qiang Gao, Hoe Hark Tan, Chennupati Jagadish and CZ Ning, *Nano Letters* 2012, vol. 12, pp. 3378-3384. ;
25. Linus E Jensen, Mikael T Björk, Sören Jeppesen, Ann I Persson, B Jonas Ohlsson and Lars Samuelson, *Nano Letters* 2004, vol. 4, pp. 1961-1964. ;
26. JWW Van Tilburg, RE Algra, WGG Immink, M Verheijen, EPAM Bakkers and Leo P Kouwenhoven, *Semiconductor Science and Technology* 2010, vol. 25, p. 024011.
27. Feng Ning, Li-Ming Tang, Yong Zhang and Ke-Qiu Chen, *Journal of Applied Physics* 2013, vol. 114, p. 224304.
28. Haibo Shu, Dan Cao, Pei Liang, Shangzhong Jin, Xiaoshuang Chen and Wei Lu, *The Journal of Physical Chemistry C* 2012, vol. 116, pp. 17928-17933. ;
29. M Galicka, M Bukała, R Buczko and P Kacman, *Journal of Physics: Condensed Matter* 2008, vol. 20, p. 454226.
30. Haibo Shu, Xiaoshuang Chen, Huxian Zhao, Xiaohao Zhou and Wei Lu, *The Journal of Physical Chemistry C* 2010, vol. 114, pp. 17514-17518.
31. H. J. Joyce, J. Wong-Leung, Q. Gao, H. Hoe Tan, and C. Jagadish, *Nano Letters*, 2010. **10**(3): p. 908-915.
32. S. Cahangirov and S. Ciraci, *Physical Review B*, 2009. **79**(16): p. 165118-1 - 165118-8.
33. Xiangyang Huang, Eric Lindgren and James R Chelikowsky, *Physical Review B* 2005, vol. 71, p. 165328.
34. Pedram Razavi and James C Greer, *Materials Chemistry and Physics* 2018, vol. 206, pp. 35-39.
35. Koichi Momma and Fujio Izumi, *Journal of Applied Crystallography* 2011, vol. 44, pp. 1272-1276.

Figure 1. Structure of (a) [100]-oriented, (b) [110]-oriented, and (c) [111]-oriented InAs and GaAs nanowires used in this work. Green spheres are In/Ga, purple spheres are As, and grey spheres schematically indicate surface passivation for the terminating groups –pseudo-H, -H, - F, and -NH_2. Images rendered using VESTA [35].

Figure 2. One-dimensional band structure (DFT/GGA) for (a) [100]-oriented GaAs and (b) [100]-oriented InAs nanowire and (c) [111]-oriented InAs nanowire using H-terminations. The length of the side of the approximately square cross section of the nanowires are 1.6 nm, 2.0 nm and 3.0 nm, respectively, and energies are referenced with respect to the valence band edge.

Figure 3. One-dimensional band structure (DFT/GGA) for [100]-oriented InAs nanowires with (a) Pseudo-H, (b) -H, (c) -NH_2, and (d) -F terminations. The nanowire core diameter is 1.2 nm and energies are referenced with respect to the valence band edge.

Figure 4. (a) Band gap energy from DFT/GGA and hybrid (HSE06) calculations and (b) effective masses at conduction band edge from DFT/GGA calculations for the [100]-oriented InAs NW as a function of the nanowire thickness (length of a side) for various surface terminations.

Figure 5. Partial density of states (PDOS) for the 1.2 nm [100]-oriented InAs NWs with different surface terminations decomposed into contributions of core In-As nanowire (solid lines) and the surface passivating species (-X) (dash lines). Energies are referenced with respect to the conduction band edge.

Supplementary Material for:

Influence of Surface Passivation on Indium Arsenide Nanowire Band Gap Energies

Pedram Razavi[1] and James C. Greer[2*]

[1]Tyndall National Institute, University College Cork, Lee Maltings, Dyke Parade, Cork T12 R5CP, Ireland

[2]University of Nottingham Ningbo New Materials Institute and Department of Electrical and Electronic Engineering, University of Nottingham Ningbo China, 199 Taikang East Road, Ningbo 315100, China

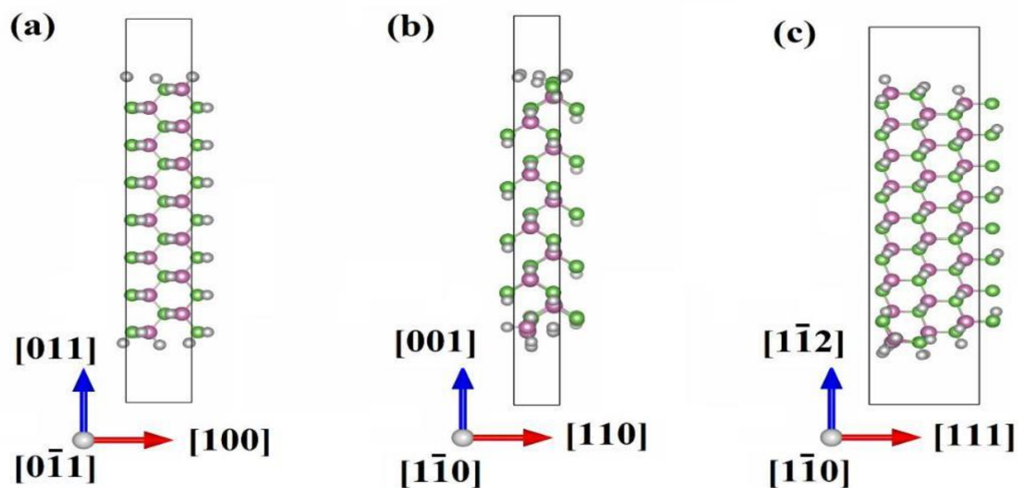

Figure S1. Side view of the structure of (a) [100]-oriented, (b) [110]-oriented, and (c) [111]-oriented InAs and GaAs nanowires used in this work. Green spheres are In/Ga, purple spheres are As, and grey spheres schematically indicate surface passivation for the terminating groups –pseudo-H, -H, -F, and -NH_2. Images rendered using VESTA [33].

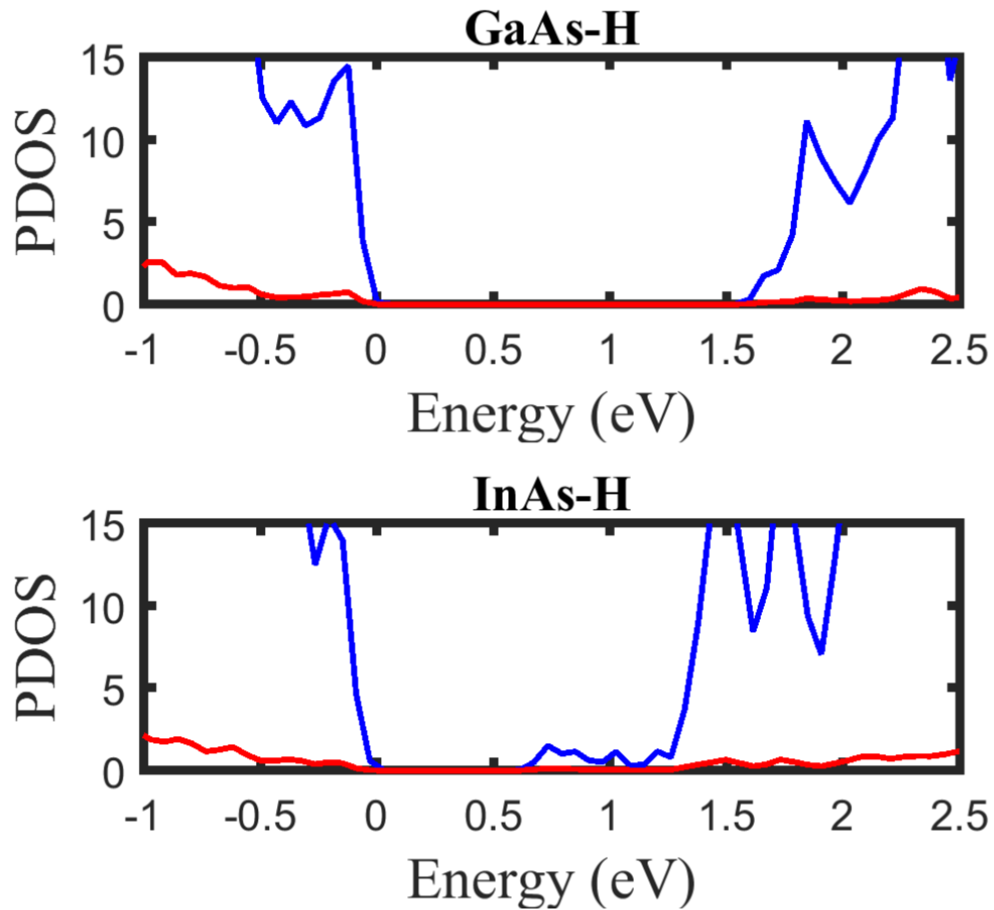

Figure S2. Projected density of states (PDOS) for the (a) 1.6 nm [100]-oriented GaAs NWs and (b) 2.0 nm [100]-oriented InAs NWs with -H surface terminations. The DoS of states is decomposed into contributions of core In-As nanowire (blue) and the surface passivating species (red) . Energies are referenced with respect to the conduction band edge.

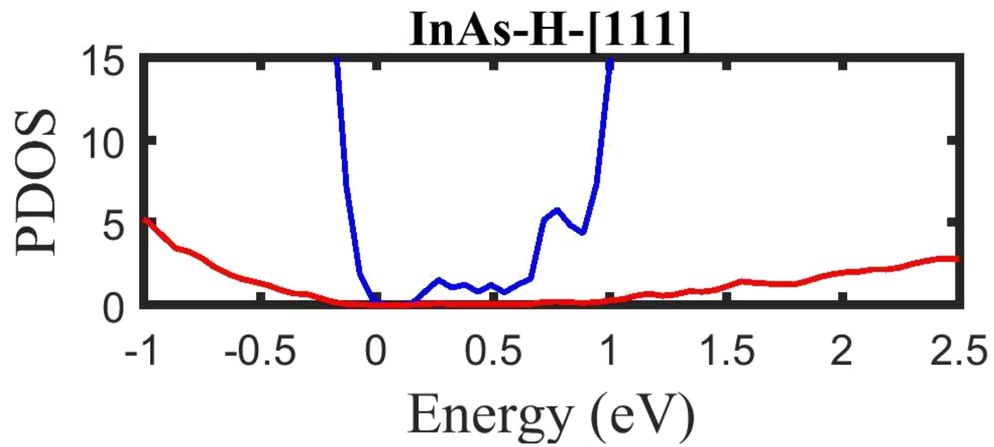

Figure S3. Projected density of states (PDOS) for the 3.0 nm [111]-oriented InAs NWs with -H surface terminations with the DoS decomposed into contributions of the core In-As nanowire (blue) and the surface passivating species (red). Energies are referenced with respect to the conduction band edge.